Supporting Information

Raney et al. 10.1073/pnas.1604838113

Experiments

Fabrication. The structures were produced using direct ink writing, an extrusion-based 3D printing method, followed by an infilling step. A viscoelastic polydimethylsiloxane (PDMS) ink was used for 3D printing. This consisted of a shear-thinning PDMS material, Dow Corning SE-1700 (85 wt %), with a lower-viscosity PDMS additive, Dow Corning Sylgard 184 (15 wt %). The viscoelastic yield properties are tailored (see supporting information in ref. 5 for rheological characterization) to ensure that the uncured ink both flows readily during printing, yet maintains its shape until it is permanently cross-linked in a subsequent curing step (100° C for 30 min). This material was extruded through a tapered nozzle (200 μm inner diameter tapered nozzle from Nordson EFD) during programmed translation of the nozzle over a fixed substrate (PTFE-coated aluminum). Ink extrusion was controlled via fixed pressure (Nordson EFD Ultimus V pressure box), with the nozzle precisely positioned using a custom 3D positioning stage (Aerotech). After printing and curing of the PDMS ink, two regions parallel with and adjacent to the functional region of wave propagation were infilled with epoxy (Momentive Epon 828) to prevent undesired structural bending that would make measuring the response of the system difficult. The lateral distance between these rigid supports, d, is defined by acrylic braces of precise dimensions, which were made using an Epilog Laser Mini cutting system. The acrylic braces also serve to elevate the soft structure (via the epoxy supports) without contacting it, to eliminate any interactions between the wave pulse and the table surface. A cylindrical copper rod (3.175 mm diameter) was cut to pieces of 5.17 mm length (giving a mass of ∼0.47 g), which were press fit into the printed structure to enable optical tracking of periodic points along the structure. The top surfaces of these copper cylinders were painted with flat white paint to produce excellent light contrast for visualization of the transition wave propagation.

To achieve a range of effective stiffnesses k, several different geometries were designed for the linear coupling elements that connect the individual bistable elements to one another. As shown in Fig. S1, we measured stiffness values ranging from 30 to 2,100 N/m (as measured with a commercial quasistatic test system, Instron 5566, in displacement control at a displacement rate of 2 mm/min). Additional intermediate values can be obtained by varying the translation speed of the printhead during the printing process.

Small-Amplitude Excitation. To characterize the dynamic response of the system, we considered small-amplitude excitations with white noise up to 5 kHz generated by an electrodynamic shaker (model K2025E013; Modal Shop) directly connected to one end of the sample. We monitored the propagation of the mechanical signal using two miniature accelerometers (352C22; PCB Piezotronics) attached to both ends of the chain (Fig. S2*A*). Spectra were obtained for three different chain lengths (6, 15, and 50 bistable units in length) and were determined to be independent of d. The rigid epoxy supports were held apart at fixed distances by acrylic braces. These ensured that the morphology of the soft structure remained in a controlled configuration during the dynamic tests. The acrylic braces were in turn glued to steel laboratory stands on an optics table, to minimize undesired vibrations. As expected for a soft, dissipative material, the transmittance spectra [defined as the ratio between the measured output and input accelerations, $A_{\text{out}}(\omega)/A_{\text{in}}(\omega)$] clearly indicate that small-amplitude excitations are rapidly dissipated due to the strong damping intrinsic to the material (Fig. S2*B*). In fact, at frequencies above 550 Hz, all energy is essentially dissipated before traveling through only six bistable units (independently of the direction of transmission or the state of the bistable elements). For longer distances (50–100 repeating units), even lower frequencies (100 Hz or less) show a drop of at least 20 dB through the structure, meaning that no more than about 1% of the input acceleration is measured at the output for these low frequencies. These results confirm that the material from which the medium is architected is intrinsically highly dissipative and does not enable propagation of small-amplitude elastic waves over long distances.

Measuring Transition Waves. Measurements of the transition waves were made using a high-speed camera (Phantom v7.1). For systems with low wave speeds (usually $k = 80$ N/m and v on the order of a few meters per second), a 500-Hz recording rate was used. For higher-speed systems (usually $k = 2{,}100$ N/m and v between 10 and 20 m/s) a higher recording rate of 1,000 Hz was used. Two halogen floodlights were positioned to provide sufficient lighting for the high-speed camera to record the experiments solely with light reflected from the sample. After recording the wave experiment with the high-speed camera, custom code in MATLAB was used to track the locations of each bistable element, allowing the output of the positions for each element i for all time, $x_i(t)$.

Control of Wave Propagation. Although the results reported in Fig. 3 were obtained numerically, we also experimentally characterized the propagation of large-amplitude waves in systems characterized by different values of k and d.

First, to validate the numerical predictions for the on-site potential, we performed quasistatic 1D displacement-controlled experiments for different d values on an individual bistable element. The experimental results reported in Fig. S5 show a convincing agreement with the numerical results (Fig. 3*A*).

Next, we experimentally investigated the effect of d and k on both wave velocity and pulse width.

To explore the effect of d on the wave behavior, we tested the propagation of a transition wave through a system in which different values of d were assigned for the different experiments (Fig. S6). This can be done without fabricating a new sample for each experiment because different values of d can be achieved by applying a defined lateral displacement ($d = 17.5$ and 18.6 mm in Fig. S6). Comparison between the experimental results shows an evident change in slope of the interface between the pretransitioned and posttransitioned states (blue and red, respectively), indicating a variation in pulse velocity (the slope of the interface is inversely proportional to the speed). In particular, we observe a change in the wave speed from about 1.9 to 3.4 m/s for $d = 17.5$ mm and $d = 18.6$ mm, respectively, in a system for which $k = 80$ N/m. In contrast, it is apparent that the pulse width is not significantly affected by d, as the number of bistable elements in the midst of transitioning between solid blue and solid red remains approximately constant as a function of time.

The stiffness of the linear connecting elements, k, also greatly affects the pulse propagation. Fig. S8 *A* and *B* show data for an experiment conducted on a system with stiff and soft connecting elements (2,100 N/m and $k = 80$ N/m, respectively; Fig. S8*C*, *Insets*). First, by comparing the slope of the boundaries in Fig. S8 *A* and *B*, it is evident that the stiffness of the connecting elements affects the pulse velocity. In fact, we find velocities of ∼18 and 3.4 m/s for $k = 2{,}100$ N/m and $k = 80$ N/m, respectively. Moreover, k strongly affects the pulse width (i.e., the number of bistable elements that at any given time are simultaneously in the process of transitioning between stable states). This is evident in Fig. S8*C*,

where we compare experimental snapshots of $\hat{S}_i$ for the two systems and observe widths of ~25 and 4 elements for $k = 2{,}100$ N/m and $k = 80$ N/m, respectively.

Simulations

Computation of the On-Site Potential. One bistable beam element consists of two inclined beams with a mass placed at the center. Because the mass is rigid compared with the compliant beams, it is assumed that the force on the mass by the bistable structure is produced solely by the deformation of the beams. Due to the symmetry of the structure, the quasistatic deformation of only one tilted beam was modeled with appropriate boundary conditions. The beam was modeled using slender corotational beam finite elements (36) whose one-dimensional stretching and bending deformation are governed by a nonlinear Neo-Hookean material model with an initial slope of $E = 1.8$ MPa. Results of an example simulation are shown in Fig. S3*A*. The undeformed beam is first subjected to an initial vertical precompression v_0 according to the d value. The boundary node B is then displaced horizontally from one stable point to another in displacement control and the resulting force required is recorded. The force–displacement function obtained in this way is fit with a seventh-order polynomial. The force–displacement polynomial is validated by comparison with the experimentally measured force–displacement curve for $d = 17.5$ mm, as shown in Fig. S5*B*; note that the computed forces are multiplied by 2 to account for the force of one bistable element containing two tilted beams. This simulation was repeated for different d values to compute $V(x, d)$.

Parameters. The mass at each node was 0.419 g, with k ranging from 50 to 2,500 N/m and d ranging from 14.5 to 19.0 mm with $d = 19.0$ mm corresponding to the undeformed state, and the dissipation parameter of 0.08 N.s/m optimized by matching the computational and experimental velocity at $(k, d) = (80$ N/m, 17.5 mm) (see Fig. S4 for the comparison of experimental and simulation results by which the dissipation parameter was determined).

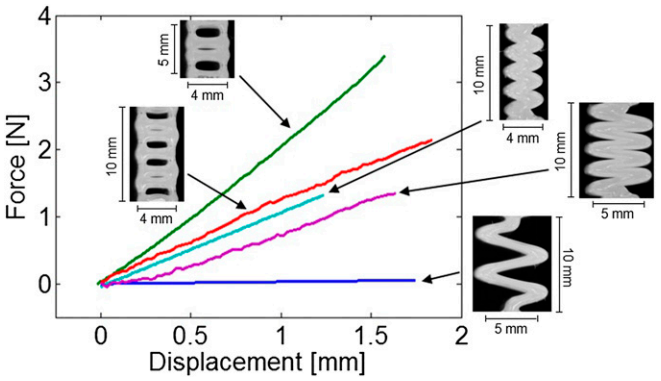

Fig. S1. Using different geometries for the linear coupling elements leads to different effective spring stiffnesses, which greatly affect the width and velocity of the propagating pulse. The stiffnesses were measured using an Instron 5566 in displacement control with a rate of 2 mm/min. The measured stiffnesses of the linear elements shown here were measured to vary from 30 to 2,100 N/m.

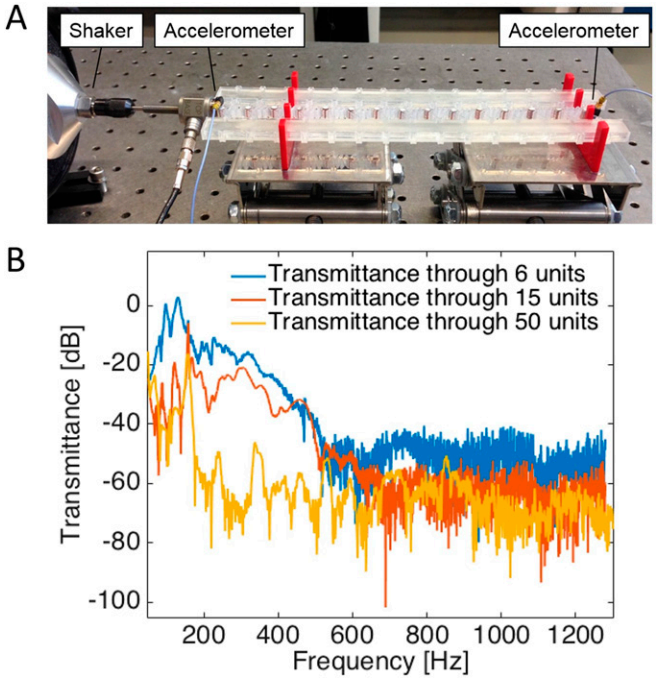

Fig. S2. (*A*) The shaker (on the left) was attached to an accelerometer that was directly glued to the samples. The accelerator used to measure the output was glued to the other end of the sample. The acrylic braces (red) were used to hold the soft architecture at well-defined widths and were glued to the laboratory stands to prevent unwanted movement. (*B*) Small-amplitude, linear excitation from either end of the chain is rapidly dissipated due to the damping intrinsic to the polymer, as is particularly evident with increasing frequency, shown here for samples with 6, 15, and 50 bistable units.

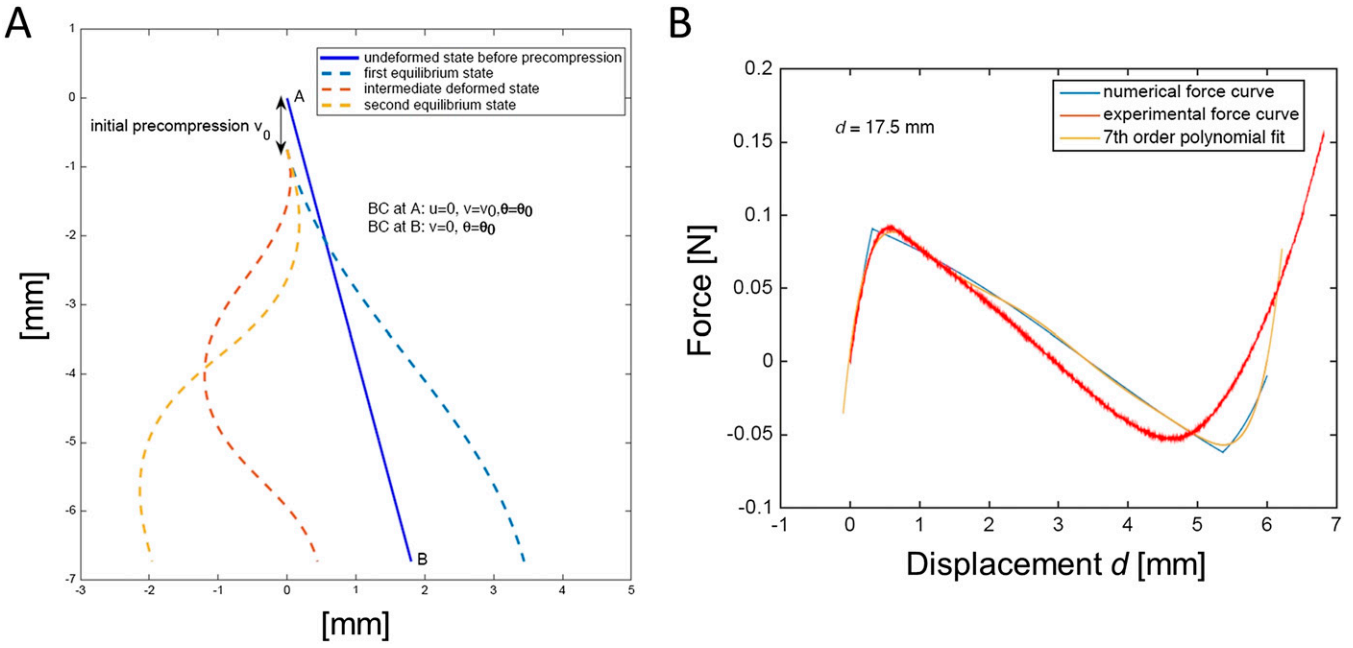

Fig. S3. (*A*) An example of the beam deformation simulation is shown. All simulations were performed on only one half of the bistable element (i.e., on one tilted beam). Different configurations of the beam are shown as it is displaced from one stable configuration to another. The force at node B is measured (and doubled to account for bistable element consisting of two tilted beams). (*B*) The numerical, experimental, and best-fit force–displacement curves are shown for $d = 17.5$ mm. The graphics indicate that experimental and numerical results are in good agreement.

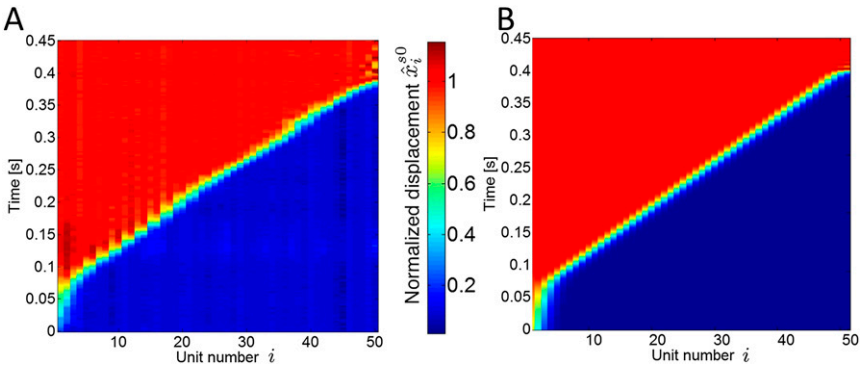

Fig. S4. (*A*) Experimental and (*B*) simulation results corresponding to (k, d) = (80 N/m, 17.5 mm), as used to determine the dissipation parameter in the model.

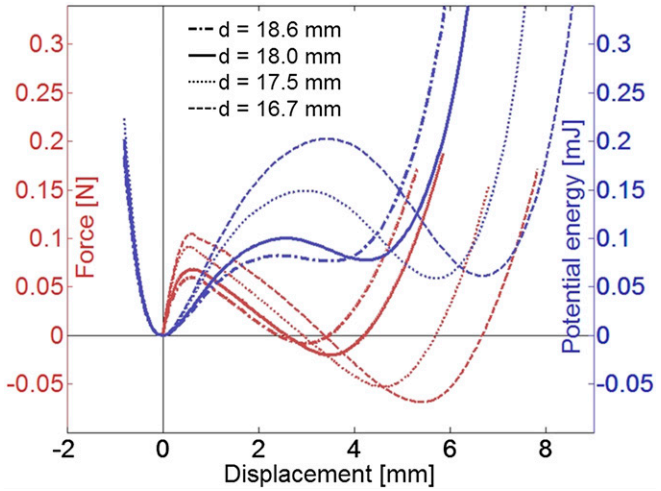

Fig. S5. Experimental data obtained by directly measuring the force–displacement behavior of a single bistable element for different lateral constraints, *d*. The potential energy is calculated from this, showing a large effect of *d* on the energy barrier of the bistable elements.

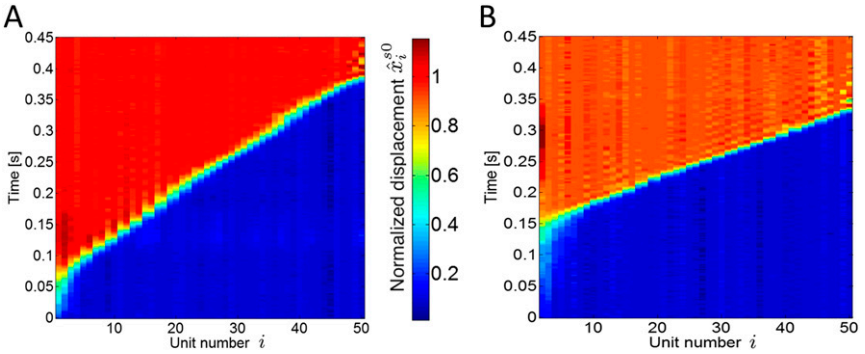

Fig. S6. (*A*) Experiments show that when *d* is small (17.5 mm here), the energy barrier between the two stable states is larger, and the wave propagation is slower. (*B*) When *d* is larger (18.6 mm here), the smaller energy barrier allows a larger propagation speed, as evidenced by the changed slope.

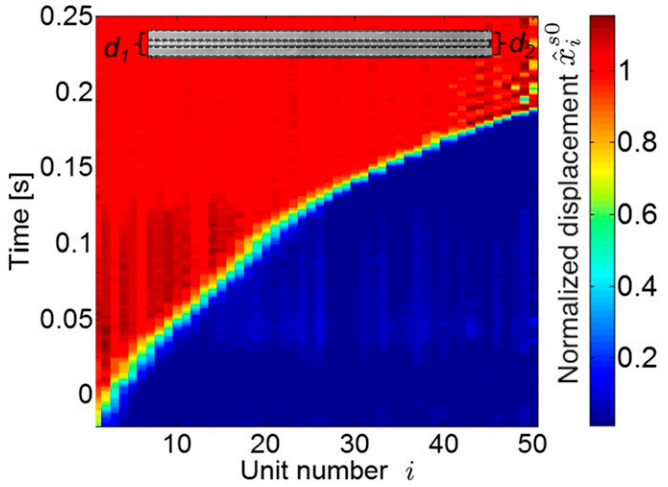

Fig. S7. Because the system is deformable, different values of *d* can be used along the length of the system, resulting in spatially varying energy barriers to propagation; this can be used to vary the velocity along the length of the chain, as it is here for a gradient structure (*d* is about $d_1 = 14.5$ mm at the left end and about $d_2 = 19.0$ mm at the right end, corresponding to measured speeds of 0.8 and 5.2 m/s, respectively).

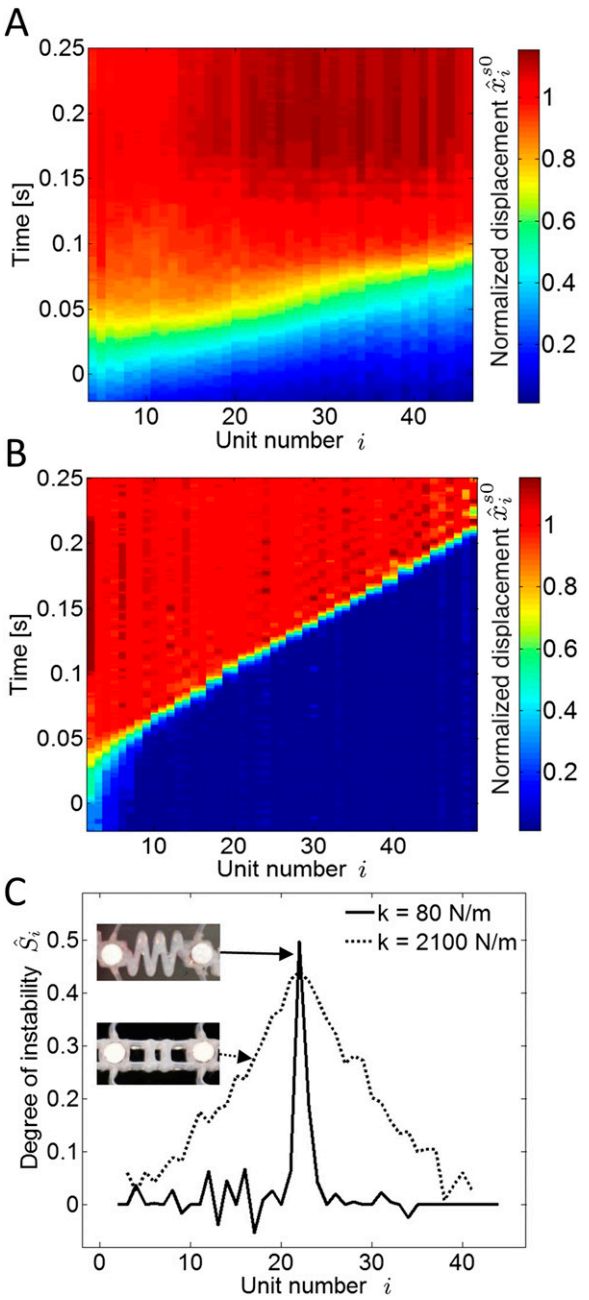

Fig. S8. (*A*) When *k* is high (2,100 N/m here), experiments show that both the pulse width and the pulse velocity (as determined by the slope) are much higher, even with the same value of *d* (18.6 mm), than (*B*) when *k* is low (80 N/m here). (*C*) The same comparison can be made by taking experimental snapshots of the two different systems (k = 80 N/m and k = 2,100 N/m, corresponding to the differences in morphology of these elements, as pictured in *Insets*).

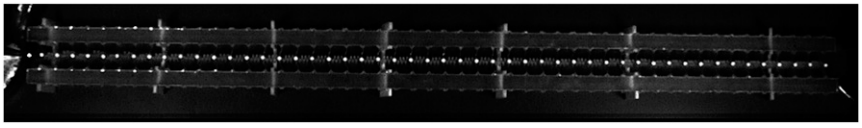

Movie S1. An example raw movie of a propagation event ($d = 18.6$ mm, $k = 80$ N/m) as filmed via a high-speed camera (Phantom v7.1) at 500 Hz and replayed at 25 Hz.

Movie S1

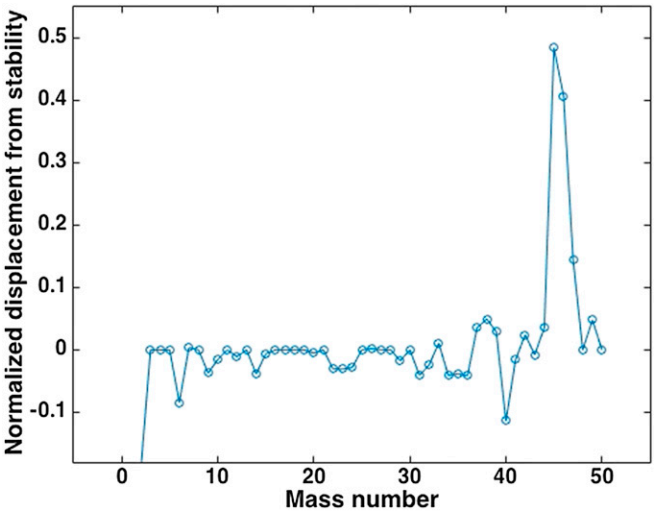

Movie S2. The propagation event from Movie S1, with the locations of the individual bistable elements tracked. The quantity being plotted is $\hat{S}_i$, the minimum normalized distance to the nearest stable configuration for each of the i bistable elements.

Movie S2

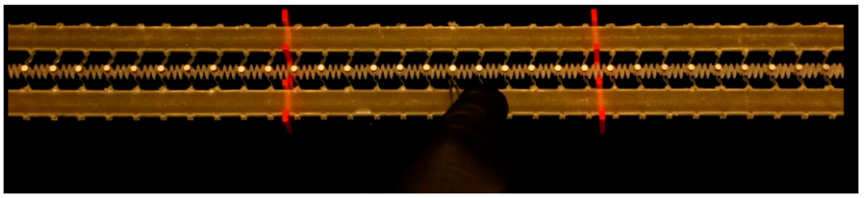

Movie S3. A propagation event recorded in real time for which propagation is initiated in the center of the system, resulting in the propagation of a tensile pulse in one direction and a compressive pulse in the other direction (with equal speed and pulse width).

Movie S3

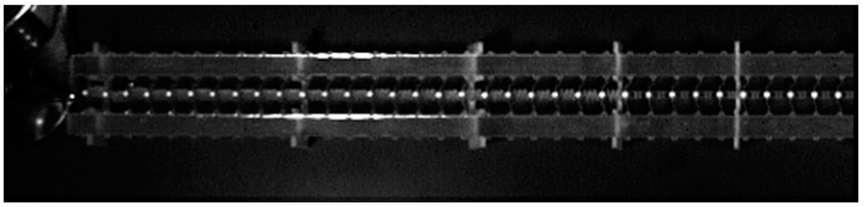

Movie S4. High-speed camera movie of diode behavior in a heterogeneous system ($k = 80$ N/m on the left and $k = 2{,}100$ N/m on the right of the system). The pulse is initiated in the soft region on the left and does not have sufficient energy to propagate into the stiff region on the right.

Movie S4

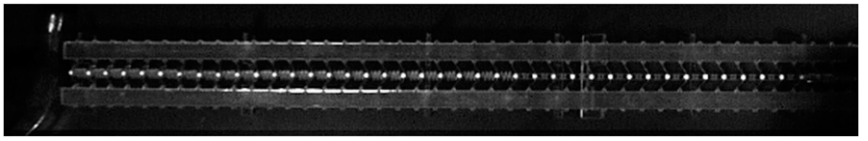

Movie S5. The same heterogeneous system of Movie S4 but now with a pulse initiated in the stiff region on the right. The pulse has sufficient energy to pass through the interface and through the soft region on the left.

Movie S5

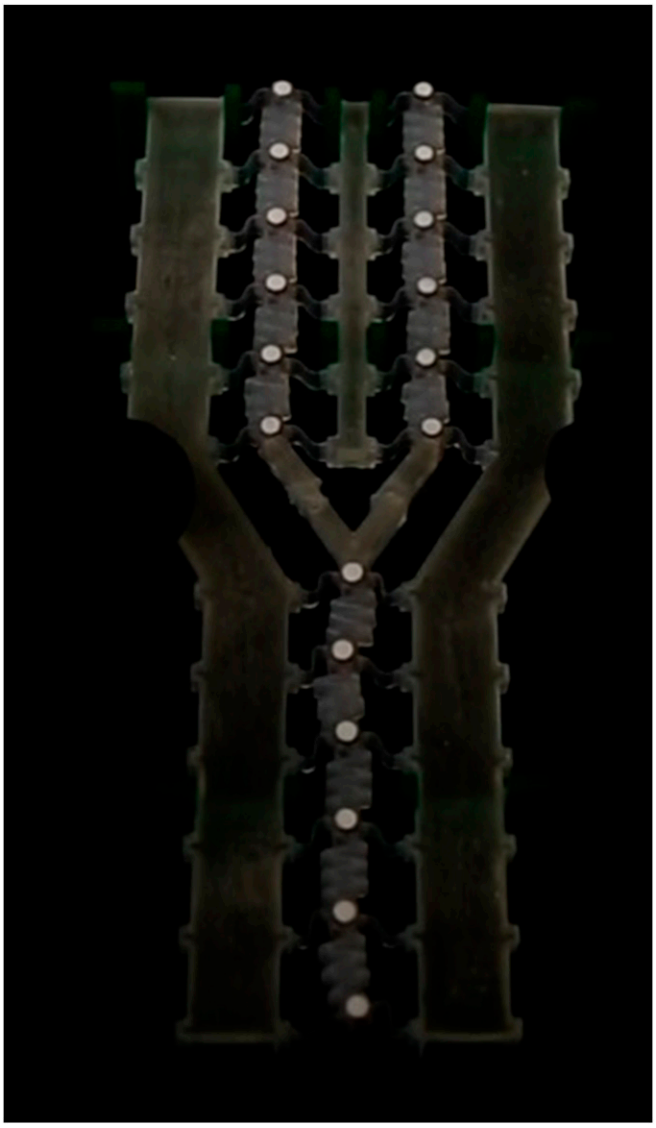

Movie S6. A bifurcated system in which functional "and" behavior is realized through the control of the spacing in the output chain ($d_{out} = 16.7$ mm). Both input chains must be activated in order for a pulse to propagate in the output chain.

Movie S6

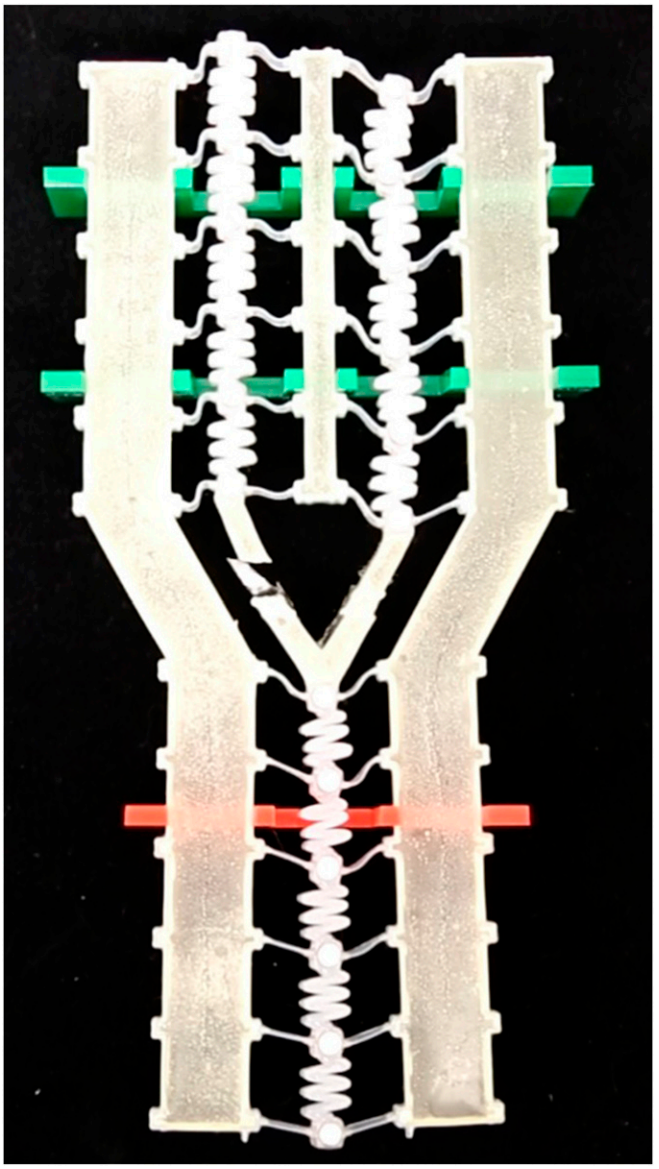

Movie S7. The same bifurcated system as in Movie S6 but now with d_{out} increased to 18.6 mm. Because of the concomitant decrease in the energy barrier, the activation of either input chain is sufficient to continue wave propagation through the output chain (functional "or" behavior).

Movie S7